Impact of $n = 1$ field on the non-axisymmetric magnetic perturbations associated with the edge localized mode crashes in the ASDEX Upgrade tokamak

Nengchao Wang (王能超),[1, 2, *] Yunfeng Liang (梁云峰),[1, 2, 3, *] Valentin Igochine,[4] Wolfgang Suttrop,[4] Li Li (李莉),[2,5] Marc Maraschek,[4] Matthias Bernert,[4] Peter Denner,[2] Michael Faitsch,[4] Sina Fietz,[4] Yu Gao (高宇),[2] Louis Giannone,[4] Andrew Kirk,[6] Hendrik Meyer,[6] Felician Mink,[4] Paolo Piovesan,[7] the ASDEX Upgrade Team[4] and the EUROfusion MST1 Team[†]

1 International Joint Research Laboratory of Magnetic Confinement Fusion and Plasma Physics, State Key Laboratory of Advanced Electromagnetic Engineering and Technology, School of Electrical and Electronic Engineering, Huazhong University of Science and Technology, Wuhan 430074, People's Republic of China

2 Forschungszentrum Jülich GmbH, Institut für Energie- und Klimaforschung - Plasmaphysik, 52425 Jülich, Germany

3 Institute of Plasma Physics, Chinese Academy of Sciences, PO Box 1126, Hefei 230031, People's Republic of China

4 Max-Planck-Institut für Plasmaphysik, D-85748 Garching, Germany

5 College of Science, Donghua University, Shanghai 201620, People's Republic of China

6 CCFE, Culham Science Centre, Abingdon, OX14 3DB, U.K.

7 Consorzio RFX, Corso Stati Uniti 4, I-35127 Padova, Italy

In the ASDEX Upgrade tokamak, the growth of non-axisymmetric magnetic perturbation (NAMP) associated with the ELM crash events has been observed, and both the poloidal and toroidal phases of NAMPs, measured by a set of Mirnov coils, were highly random. By applying an $n = 1$ magnetic perturbation (MP) field, the phases of NAMPs were locked to the phase of the total $n = 1$ resonant MP (RMP) field, which takes the plasma response to the MP field into account. This observation can be explained by the resonant electromagnetic $\boldsymbol{J} \times \boldsymbol{B}$ torque applied by the RMP field on a magnetic island formed due to the magnetic reconnection, which is predicted to occur during the ELM crashes by several numerical modelling results.

Introduction – The edge-localized mode (ELM) [1] is characterized by a periodic fast collapse of the edge pressure associated with explosive losses of heat and particles in high confinement mode (H-mode) fusion plasmas. The ELM could significantly shorten the lifetime of the plasma facing components, thus it is of great importance to understand the ELM dynamic process and to control the peak heat flux on divertor plates for a fusion reactor like ITER [2]. The dynamics of ELM crashes, especially its three-dimensional (3D) features, have been studied extensively [3-6], however, it has not been fully understood yet [7].

Magnetic reconnection [8], which is followed by the formation of magnetic islands at the rational flux surfaces, plays a vital role for understanding the collapse events in magnetized plasmas, such as sawtooth crashes [9], minor disruptions [10] in tokamaks and solar flares [11] in the solar atmosphere. The fast energy loss during the ELM crash is also proposed to be due to magnetic reconnection [12]. Several nonlinear numerical MHD modelling codes, such as JOREK [13, 14], BOUT++ [15] and NIMROD [16], have shown the formation of magnetic islands and stochastic regions at the edge plasma during the ELM crashes. However, to date, no direct experimental evidence of magnetic reconnection has been observed during the ELM crashes.

In a toroidally symmetric tokamak plasma, the occurrence of magnetic reconnection can be identified by the formation of magnetic islands. In past tokamak experiments with lower performance

plasmas, the magnetic island structure was directly described by the radial distribution of the non-axisymmetric magnetic perturbations (NAMPs) [17] measured by magnetic probes around the rational surface. However, such measurement is difficult to apply to high temperature H-mode plasmas, where the NAMPs are normally measured by a set of magnetic probe array outside the plasma. Therefore, the time evolution of radial plasma profiles [18, 19] has been used as an assistant to the judgment of a rotating magnetic island. Recently, the external resonant magnetic perturbation (RMP) field has been widely applied to study and control the magnetic island. RMP can either induce magnetic island via forced magnetic reconnection [20, 21], or lock the phase of the magnetic island [22-25], so called the phase locking effect, via the resonant electromagnetic $J \times B$ torque [25]. The phase locking effect of the interaction between RMP and magnetic island has been applied to control the phase [26] and the rotation frequency [27] of the magnetic island, and also been considered as a typical feature for identification of magnetic islands in the tokamak plasma, such as the *locked mode* [22-25].

In this letter, we report the observations from the ASDEX Upgrade tokamak experiments on the NAMPs with low toroidal mode number growing associated with the ELM crash events, which are similar to those observed in TCV [28]. Both the poloidal and toroidal phases of NAMPs, measured by a set of Mirnov coils, were highly random. To identify the sources which produce the NAMPs, the external $n = 1$ magnetic perturbation (MP) field was applied to probe the responses of NAMPs, while maintaining the ELM frequency hardly affected. It is found that both the toroidal and poloidal phases of NAMPs are locked to the phase of the total $n = 1$ RMP field. This observation can be explained by the resonant electromagnetic $J \times B$ torque, applied by the RMP field on a magnetic island due to the magnetic reconnection, which is predicted to occur during the ELM crashes by several numerical modelling results.

Experimental setup and results – On the ASDEX Upgrade tokamak, a set of in-vessel MP coils has been applied to produce a MP field with various toroidal configurations as shown in Fig. 1 [29, 30]. In this experiment, the target type-I ELMy H-mode plasmas, *perturbed* by an $n = 1$ MP field in #31021 [31] and *unperturbed* in #31030, were operated with an edge safety factor, q_{95}, of 4.3 (plasma current of 1 MA and toroidal field of 2.58 T). The pedestal top parameters are: electron density $n_{e,ped} \sim 5 \times 10^{19}$ m^{-3}, electron temperature $T_{e,ped} = 0.8 \sim 1.1$ keV, corresponding to a moderate pedestal electron collisionality, $v_{e,ped}*$, of around 0.4. The $n = 1$ MP field was rigidly rotated at 5 Hz for the *perturbed* plasma and its toroidal phase, Φ_{MP}, is represented by the $n = 1$ phase of the currents in the upper MP coils, Φ_U, e.g. it was 304° for the case shown in Fig. 1(a).

Two poloidal and one mid-plane toroidal Mirnov coil arrays are used to identify both the amplitude and the phase of the NAMPs during ELM crashes. Here, these two poloidal Mirnov arrays are toroidally separated by 180° and each of them consists of 30 poloidally distributed Mirnov coils as shown in Fig. 1, while the toroidal array consists of four Mirnov coils unevenly distributed at the low field side with toroidal angles of $\varphi = 90^o$, 135°, 270° and 315°, respectively. The poloidal field, B_θ, is obtained by integrating the differential signals (dB_θ/dt) from each Mirnov coil. The change of B_θ during the ELM crashes has two components: *i*) the $n = 0$ part which could be induced by an inward or outward $n = 0$ equilibrium shift, and *ii*) the non-axisymmetric part which is mainly due to plasma instabilities. Hence, the $n =$ odd component of NAMPs, $b_\theta^{odd,ELM}$, is determined by taking half the difference between two B_θ signals which were measured at the locations with the same poloidal angle, but toroidally separated by 180°. The superscript 'ELM' indicates that it is the ELM associated component, which is zero before the ELM onset. Note that this analysis procedure

eliminates all the quasi-static equilibrium magnetic field and also the 5 Hz MP field. Due to a finite number of toroidally distributed Mirnov coils, the n = even component of NAMP cannot be identified directly, and it will not be discussed in this Letter. Using all of the Mirnov probes indicated in Fig. 1, both the poloidal (20 signals at $\varphi = 90^{\circ}$) and the toroidal (2 signals at $\theta \sim 0^{\circ}$) distributions of $b_\theta^{odd,ELM}$ could be obtained.
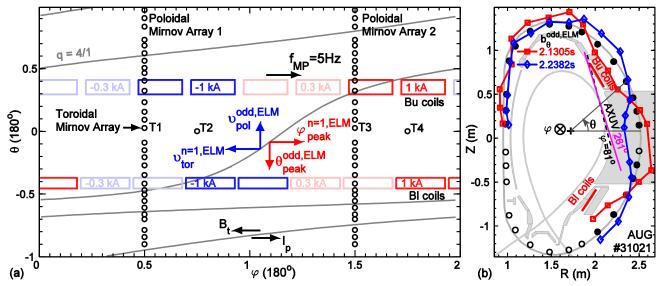

Fig. 1 (color online). (a) The toroidal arrangement of the MP coils (Bu and Bl coils) and the Mirnov probes. The propagation directions of the n = odd component of ELM associated NAMPs, $b_\theta^{odd,ELM}$, are also indicated. (b) The poloidal cross section of ASDEX Upgrade, showing the MP coils, the separatrix of the plasma in discharge 31021, two toroidal symmetric chords of the absolute extreme ultraviolet (AXUV) diodes and the poloidal Mirnov arrays (20 probes used in this experiment are filled). The poloidal distribution of $b_\theta^{odd,ELM}$ during two ELMs at 2.1305 s and 2.2382 s, as marked by the arrows in Fig. 3, are indicated by the red squares and blue diamonds in (b) respectively, with the distances between the marker and the corresponding Mirnov coil proportional to the measured $b_\theta^{odd,ELM}$. The toroidal and poloidal direction are defined in (b), with the plasma current (I_p) in $+\varphi$ direction and the toroidal field (B_T) in $-\varphi$ direction.
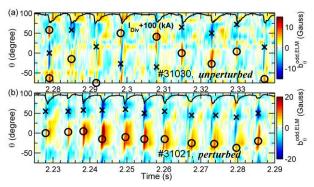

Fig. 2 (color online). Comparison of the poloidal distribution of $b_\theta^{odd,ELM}$ for the (a) *unperturbed* and (b) *perturbed* plasmas by the n = 1 MP field. The tile currents measured in the outer divertor, I_{Div}, are plotted in black lines as an indicator of the ELM crashes. The circles and crosses mark the peaks and dips of NAMPs respectively.
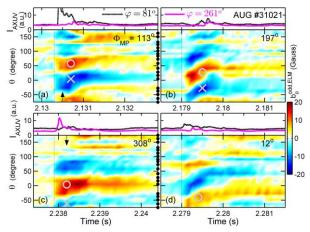

Fig. 3 (color online). Contours of $b_\theta^{odd,ELM}$ vs θ and time and the waveforms of two AXUV signals, measured at $\varphi = 81^{\circ}$ and 261°, during four ELMs with different Φ_{MP} in discharge 31021. The black dots in the right of (a) and (c) indicate the poloidal locations of the measurement, while the vertical dashed lines indicate the ELM onset. The two black arrows mark the times of the poloidal distributions of $b_\theta^{odd,ELM}$ shown in Fig. 1(b).

Fig. 2 shows a comparison of the NAMPs, indicated by $b_\theta^{odd,ELM}$, in the *unperturbed* and *perturbed* plasmas by the n = 1 MP field. The negative bursts observed in the tile currents measured in the outer divertor (I_{Div}, black lines) indicate the onset of ELM crashes [32]. Accompany with the ELM crash,

there is a clear mode structure characterized with peaks and dips in the poloidal profile of NAMPs. This mode structure disappeared shortly after the ELM crash in the *unperturbed* plasma, while it remained in the *perturbed* plasma for a few milliseconds. Interestingly, the peaks and dips of NAMPs appeared almost at fixed poloidal locations if *perturbed* (marked by the black circles and crosses in Fig. 2 (b)), while they appeared at more random poloidal locations if *unperturbed* (Fig. 2 (a)).

The different behaviors of NAMPs observed in the *perturbed* and *unperturbed* plasmas indicates that the NAMPs responded to the applied $n = 1$ MP field. In Fig. 3, a detailed time evolution of NAMPs at four different Φ_{MP} is shown. By tracing the peak/dip trajectory, it is found that the ELM associated mode structure propagated poloidally in the electron diamagnetic drift direction in the laboratory frame during each individual ELM, and then stayed at a constant location before it decayed away. In addition, the phase of NAMPs was changed roughly by 180° when Φ_{MP} increased by around 180°. A direct comparison of NAMPs observed during applications of the $n = 1$ MP field with two opposite phases was also shown in Fig. 1 (b). This indicates that the poloidal phase of NAMPs was strongly impacted by the $n = 1$ MP field.

The amplitude and toroidal phase of NAMPs can be calculated by fitting the two $b_\theta^{odd,ELM}$ signals from the toroidal array against their toroidal locations using a sine function and a known toroidal mode number. It has been observed previously that low n modes, dominated by $n = 1$ or 2 component, grow non-linearly before and during the ELM crashes in AUG [33] and TCV [28]. Considering that the $n = 1$ MP field affected the poloidal phase of $b_\theta^{odd,ELM}$ as described above, the assumption that the measured $b_\theta^{odd,ELM}$ consists mainly of the $n = 1$ component has been adopted. Fig. 4 displays the calculated amplitudes and toroidal phases of the $n = 1$ component of NAMPs ($b_\theta^{n=1,ELM}$ and $\varphi^{n=1,ELM}$).
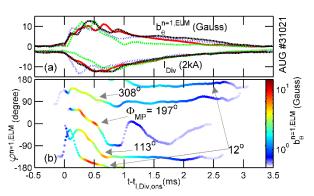

Fig. 4 (color online). The evolution of (a) the amplitudes and (b) the toroidal phases of the $n = 1$ component of NAMPs for the four ELMs shown in Fig. 3. $b_\theta^{n=1,ELM}$ is also indicated by the color scale in (b). The time with respect to the ELM onset ($t_{I,Div,ons}$, as marked in Fig. 3) are used.
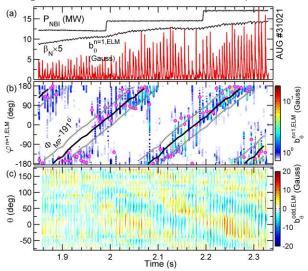
Fig. 5 (color online). The evolution of (a) the NBI power, β_N, $b_\theta^{n=1,ELM}$, (b) the $\varphi^{n=1,ELM}$, $\varphi^{n=1,ELM}_{peak}$ (magenta dots corresponding to 78 ELMs), Φ_{MP} -191°, and (c) the poloidal distribution of $b_\theta^{odd,ELM}$. The color scale indicates (b) $b_\theta^{n=1,ELM}$ and (c) $b_\theta^{odd,ELM}$. The solid line in (b) indicates that $\varphi^{n=1,ELM}_{peak} = \Phi_{MP}$ -191°, while the dashed lines mark the one standard deviation region ($\sigma = 47^o$).

Fig. 5 shows the evolution of NAMPs with stepping up of the NBI power, while the ECRH power is around 1.4 MW. With the rise of β_N, $b_\theta^{n=1,ELM}$ is also observed to increase, while $\varphi^{n=1,ELM}$ shows a

clear shift towards the co-I_p direction with the rotation of the $n = 1$ MP field. Especially, the $\varphi^{n=1,ELM}$ measured at the peak of $b_\theta^{n=1,ELM}$ during each ELM ($\varphi^{n=1,ELM}_{peak}$, Fig. 5(b)) was linear to Φ_{MP}. As a comparison, the $\varphi^{n=1,ELM}_{peak}$ in the *unperturbed* plasma is highly random, similar as the corresponding poloidal phase. The poloidal distribution of $b_\theta^{odd,ELM}$ was also modulated by the 5 Hz rotating $n = 1$ MP field (Fig. 5 (c)). The poloidal phase at the peak of $b_\theta^{odd,ELM}$, $\theta^{odd,ELM}_{peak}$, was shifted towards $-\theta$ direction, which corresponds to the ion diamagnetic drift direction and is the same as the rotation direction of the $n = 1$ MP field (Fig. 1(a)). These observations reflect that both the toroidal and poloidal phases of NAMPs can be locked to the externally applied $n = 1$ MP field.

The toroidal velocity of the ELM associated mode structure is observed to be around a few km/s in the counter-I_p direction in the LFS mid-plane, e.g. $\upsilon_{tor}^{n=1,ELM} \sim -10.3$ km/s for the NAMP at $\Phi_{MP} = 113°$ shown in Fig. 4. In the NBI driven fast rotating plasma, this mode structure could be only localized at the plasma edge. This reflects the formation of 3D perturbed currents at the edge of the plasma during the ELM crash events, and their phases could be locked to the externally applied MP fields. Meanwhile, the toroidal asymmetry of the edge AXUV radiation, I_{AXUV}, has been measured during the ELM crashes by two toroidal symmetric chords of the AXUV diodes [34]. This toroidal asymmetry, which might be due to the existence of the NAMP, can be impacted by the $n = 1$ MP field, as shown by the four examples in Fig. 3.

The phase locking of NAMPs to $n = 1$ field can reflect the essential nature of NAMPs. The NTV torque [35] generated by the MP field can brake the plasma rotation, but it will not lead to the phase locking. The MP field also can not lock asymmetric structures such as SOL filaments [36]. The resonant electromagnetic $\boldsymbol{J} \times \boldsymbol{B}$ torque [25] applied by a RMP on a magnetic island has been widely shown to cause the phase locking between a RMP field and the 3D perturbed currents. This can be the reason why the phases of NAMPs were significantly impacted by the $n = 1$ MP field. At first glance, the applied $n = 1$ MP field in #31021 is vacuum non-resonant, as indicated by the misalignment between the pitch of coil currents and the pitch of $q = 4$ field lines in Fig. 1(a). However, due to the amplification of marginally-stable edge $n = 1$ kink mode in this high beta plasma [31] and the coupling effect [37], the total $n = 1$ RMP field at the rational surface was larger [31]. Besides, its phase was varied at 5 Hz, hence the NAMPs were phase locked to the total $n = 1$ RMP field.

To clarify the effect of plasma response on the total RMP field, a detailed poloidal spectrum scan of the $n = 1$ MP field has been performed with $q_{95} = 5.3$ and the total RMP field has been modelled by the MARS-F code [38] taking the plasma response into account, as shown in Fig. 6. A continuously scan of the differential phase between the upper and lower MP coils, $\delta\Phi_{UL} = \Phi_U - \Phi_L$, was carried out in discharge #32116, while fixed $\delta\Phi_{UL}$ were maintained from #32117 to #32119. Φ_U and Φ_L, were varied simultaneously at 1 Hz in opposite toroidal directions in #32116. As a result, the amplitude of the RMP field (and the spectrum of MP) in a vacuum assumption was modulated at 2 Hz (Fig. 6(a)), while the phase of the RMP field was flipped between two constants at 1 Hz (Fig. 6(b)). The $\varphi^{n=1,ELM}_{peak}$ were measured to flip between $\sim -130°$ and $\sim 70°$ when Φ_U was around $0°$ and $180°$ (Fig. 6(c)). The phase flip appeared at the phases of Φ_U (or $\delta\Phi_{UL}$) with a $\sim 40°$ (or $\sim 80°$) difference between the vacuum RMP and NAMPs. This difference is significantly reduced when taking the plasma response into account in the MARS-F modelling, as marked by the red vertical line in Fig. 6. Due to the plasma response [37, 39], the dependence of the total RMP field on Φ_U (or $\delta\Phi_{UL}$), has been shifted for around $40°$ (or $80°$) compared to that of the vacuum RMP field. This

match indicates that the phases of NAMPs are locked to the total RMP field, with only a small RMP amplitude.
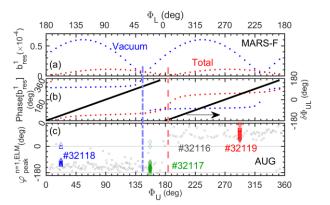

Fig. 6 The response of NAMPs to external $n = 1$ MPs at various poloidal spectrums by varying the $\delta\Phi_{UL}$ for experiments and modeling. The $\varphi^{n=1,ELM}_{peak}$ are shown in (c) for #32116 with $\delta\Phi_{UL}$ scan and from #32117 to #32119 with fixed $\delta\Phi_{UL}$. 268 ELMs from these four discharges are shown in (c). The (a) amplitude, b_{res}^1, and (b) phase, Phase[b_{res}^1], of the RMP field at $q = 7/1$ rational surface were modelled by MARS-F for vacuum (blue) and total (red) field.

Discussion and Conclusions – The phase locking of NAMPs to the total RMP field can be explained as a result of the resonant electromagnetic $\boldsymbol{J}\times\boldsymbol{B}$ torque applied by the RMP field on the magnetic island, which is measured as the NAMP. On JET, a rotating ELM postcursor mode, so called palm tree mode [40], has been observed after ELM crashes. The palm tree mode has an $n = 1$ tearing mode structure, which is consistent with our observations. On ASDEX Upgrade, the acceleration of beam ions during ELM crashes has been observed [41]. This result could be explained in terms of a resonant interaction between the fast-ion orbits and the parallel electric field emerging during the ELM, when magnetic reconnection is believed to take place. The acceleration of electrons during ELMs was also reported on MAST [42] and ASDEX Upgrade [43].

This work is also consistent with the recent JOREK modelling based on ASDEX Upgrade equilibrium, which shows that magnetic reconnection is responsible for the fast T_e collapse during ELM crash [14]. The $n = 1$ NAMPs observed in this work might be related to the important $n = 1$ component predicted by the JOREK modelling [14]. The NAMPs with $n > 1$, if exist, have not been studied in this letter due to the limitation of the diagnostic arrangement. In [14], ELM mode structures with $n = 2\sim5$ are observed experimentally at a few kilohertz during the ELM crash, via ELM synchronization of temporal Fourier analysis. They are different from the non-periodic NAMPs, which are more similar to the solitary magnetic perturbations observed previously in AUG [33] and TCV [28]. Further study on the NAMPs with $n > 1$, perhaps combined with the method used in [14], is necessary to provide a more comprehensive understanding on the ELM crashes. The phase locking of NAMPs were shown for more than 300 ELMs in this letter with a range of plasma parameters of $\beta_N = 1.8\text{-}2.8$ and $q_{95} = 4.3, 5.3$. The investigation of NAMPs behavior in a wider parameter range is also important for the future study. It is also worth noting that the magnetic island should have the same toroidal and poloidal mode numbers as the RMP field, so that the phase locking can occur.

This observation of resonant interaction between ELM and MP fields can provide the magnetic reconnection as a possible new mechanism for understanding the physics of ELM control by RMP [44, 45]. In fact, a similar differential phase shift of the total RMPs calculated in between a vacuum assumption and taking into account the plasma responses has also been observed in the experiments of ELM mitigation [39, 46] and suppression [47] using the MP field.

In conclusion, the growth of NAMPs associated with the ELM crash event has been observed on the ASDEX Upgrade tokamak. By applying an $n = 1$ MP field, the phases of NAMPs were locked to the phase of the total $n = 1$ RMP field, which takes the plasma response to the MP field into account.

This experimental observation may also be important for understanding the physics of the ELM control by RMP.

[1] H. Zohm, Edge localized modes (ELMs), Plasma Phys. Control. Fusion **38**, 105 (1996).

[2] A. Loarte *et al*., Characteristics of type I ELM energy and particle losses in existing devices and their extrapolation to ITER, Plasma Phys. Control. Fusion **45**, 1549 (2003).

[3] T. Eich *et al*., Nonaxisymmetric Energy Deposition Pattern on ASDEX Upgrade Divertor Target Plates during Type-I Edge-Localized Modes, Phys. Rev. Lett. **91**, 195003 (2003).

[4] A. Wingen *et al*., Numerical Modeling of Edge-Localized-Mode Filaments on Divertor Plates Based on Thermoelectric Currents, Phys. Rev. Lett. **104**, 175001 (2010).

[5] G. S. Yun *et al*., Two-Dimensional Visualization of Growth and Burst of the Edge-Localized Filaments in KSTAR H-Mode Plasmas, Phys. Rev. Lett. **107**, 045004 (2011).

[6] A. Kirk *et al*., Evolution of Filament Structures during Edge-Localized Modes in the MAST Tokamak, Phys. Rev. Lett. **96**, 185001 (2006).

[7] A. W. Leonard, Edge-localized-modes in tokamaks, Phys. Plasmas **21**, 090501 (2014).

[8] M. Yamada *et al.*, Magnetic reconnection, Rev. Mod. Phys. **82**, 603 (2010).

[9] H. K. Park *et al.*, Comparison Study of 2D Images of Temperature Fluctuations during Sawtooth Oscillation with Theoretical Models, Phys. Rev. Lett. **96**, 195004 (2006).

[10] Y. Liang *et al.*, Observations of secondary structures after collapse events occurring at the q = 2 magnetic surface in the TEXTOR tokamak, Nucl. Fusion **47**, L21 (2007).

[11] J. W. Cirtain *et al.*, Energy release in the solar corona from spatially resolved magnetic braids, Nature, **493**, 501 (2013).

[12] A. Kirk *et al.*, Recent progress in understanding the processes underlying the triggering of and energy loss associated with type I ELMs, Nucl. Fusion **54**, 114012 (2014).

[13] F. Orain *et al.*, Resistive Reduced MHD Modeling of Multi-Edge-Localized-Mode Cycles in Tokamak X-Point Plasmas, Phys. Rev. Lett. **114**, 035001 (2015).

[14] A.F. Mink *et al.*, Nonlinear coupling induced toroidal structure of edge localized modes, Nucl. Fusion **58**, 026011 (2018).

[15] X. Q. Xu *et al.*, Nonlinear Simulations of Peeling-Ballooning Modes with Anomalous Electron Viscosity and their Role in Edge Localized Mode Crashes, Phys. Rev. Lett. **105**, 175005 (2010).

[16] F. Ebrahimi, Nonlinear reconnecting edge localized modes in current-carrying plasmas, Phys. Plasmas **24**, 056119 (2017).

[17] D.C. Robinson and K. McGuire, Magnetic islands and disruptions in the TOSCA tokamak, Nucl. Fusion **19**, 115 (1979).

[18] R. Fitzpatrick, Helical temperature perturbations associated with tearing modes in tokamak plasmas, Phys. Plasmas **2**, 825 (1995).

[19] V. Igochine *et al.*, Conversion of the dominantly ideal perturbations into a tearing mode after a sawtooth crash, Phys. Plasmas **21**, 110702 (2014).

[20] Y. Kikuchi *et al.*, Forced Magnetic Reconnection and Field Penetration of an Externally Applied Rotating Helical Magnetic Field in the TEXTOR Tokamak, Phys. Rev. Lett. **97**, 085003 (2006).

[21] P. Denner *et al.*, Local measurements of screening currents driven by applied RMPs on TEXTOR, Nucl. Fusion **54**, 064003 (2014).

[22] T.C. Hender *et al.*, Effect of resonant magnetic perturbations on COMPASS-C tokamak discharges, Nucl. Fusion **32** 2091 (1992).

[23] Q. Hu *et al.*, Understanding the effect of resonant magnetic perturbations on tearing mode dynamics, Phys. Plasmas **20**, 092502 (2013).

[24] S. Fietz *et al.*, Influence of externally applied magnetic perturbations on neoclassical tearing modes at ASDEX Upgrade, Nucl. Fusion **55**, 013018 (2015).

[25] R. Fitzpatrick, Interaction of tearing modes with external structures in cylindrical geometry (plasma), Nucl. Fusion **33**, 1049 (1993).

[26] F. A. Volpe *et al.*, Avoiding Tokamak Disruptions by Applying Static Magnetic Fields That Align Locked Modes with Stabilizing Wave-Driven Currents, Phys. Rev. Lett. **115**, 175002 (2015).

[27] Q. Hu *et al.*, Influence of rotating resonant magnetic perturbations on particle confinement, Nucl. Fusion **54**, 122006 (2014).

[28] R. P. Wenninger *et al.*, Non-linear magnetic perturbations during edge-localized modes in TCV dominated by low n mode components, Nucl. Fusion **53**, 113004 (2013).

[29] W. Suttrop *et al.*, First Observation of Edge Localized Modes Mitigation with Resonant and Nonresonant Magnetic Perturbations in ASDEX Upgrade, Phys. Rev. Lett. **106**, 225004 (2011).

[30] W. Suttrop *et al.*, Mitigation of edge localised modes with magnetic perturbations in ASDEX Upgrade, Fusion Engineering and Design **88**, 446 (2013).

[31] P. Piovesan *et al.*, Impact of ideal MHD stability limits on high-beta hybrid operation, Plasma Phys. Control. Fusion **59**, 014027 (2017).

[32] E. Wolfrum *et al.*, Pedestal Studies at ASDEX Upgrade, in Proc. 22nd Int. Conf. on Fusion Energy (Geneva, Switzerland, 2008), paper EX/P3-7.

[33] R.P. Wenninger *et al.*, Solitary magnetic perturbations at the ELM onset, Nucl. Fusion **52**,114025 (2012).

[34] M. Bernert *et al.*, Application of AXUV diode detectors at ASDEX Upgrade, Rev. Sci. Instrum. **85**, 033503 (2014).

[35] K.C. Shaing, K. Ida and S.A. Sabbagh, Neoclassical plasma viscosity and transport processes in non-axisymmetric tori, Nucl. Fusion **55**, 125001 (2015).

[36] A. J. Thornton *et al.*, The effect of resonant magnetic perturbations on the divertor heat and particle fluxes in MAST, Nucl. Fusion **54**, 064011 (2014).

[37] D. A. Ryan *et al.*, Toroidal modelling of resonant magnetic perturbations response in ASDEX-Upgrade: coupling between field pitch aligned response and kink amplification, Plasma Phys. Control. Fusion **57**, 095008 (2015).

[38] Y. Q. Liu and A. Bondeson, Feedback stabilization of nonaxisymmetric resistive wall modes in tokamaks. I. Electromagnetic model, Phys. Plasmas **7**, 3681 (2000).

[39] L. Li *et al.*, Modelling plasma response to RMP fields in ASDEX Upgrade with varying edge safety factor and triangularity, Nucl. Fusion **56**, 126007 (2016).

[40] H. R. Koslowski *et al.*, Observation of the palm tree mode, a new MHD mode excited by type-I ELMs on JET, Nucl. Fusion **45**, 201 (2005).

[41] J. Galdon-Quiroga *et al.*, Beam-Ion Acceleration during Edge Localized Modes in the ASDEX Upgrade Tokamak, Phys. Rev. Lett. **121**, 025002 (2018)

[42] S. J. Freethy *et al.*, Electron Kinetics Inferred from Observations of Microwave Bursts During Edge Localized Modes in the Mega-Amp Spherical Tokamak, Phys. Rev. Lett. **114**, 125004 (2015).

[43] M. Willensdorfer *et al*., Dynamics of ideal modes and subsequent ELM crashes in 3D tokamak geometry from external magnetic perturbations, Plasma Phys. Control. Fusion *accepted*

[44] T. E. Evans *et al*., Suppression of Large Edge-Localized Modes in High-Confinement DIII-D Plasmas with a Stochastic Magnetic Boundary, Phys. Rev. Lett. **92**, 235003 (2004).

[45] Y. Liang *et al*., Active Control of Type-I Edge-Localized Modes with n = 1 Perturbation Fields in the JET Tokamak, Phys. Rev. Lett. **98**, 265004 (2007).

[46] A. Kirk *et al.*, Effect of resonant magnetic perturbations on low collisionality discharges in MAST and a comparison with ASDEX Upgrade, Nucl. Fusion **55**, 043011 (2015).

[47] C. Paz-Soldan *et al*., Observation of a Multimode Plasma Response and its Relationship to Density Pumpout and Edge-Localized Mode Suppression, Phys. Rev. Lett. **114**, 105001 (2015).